JMEPEG (2012) 21:2487–2494
DOI: 10.1007/s11665-012-0206-3

1059-9495/$19.00

Microstructural Characterization of Co-Based ODS Alloys

Lin Zhang, Xuanhui Qu, Xinbo He, Rafi-ud Din, Hengsan Liu, Mingli Qin, and Hongmin Zhu

(Submitted July 31, 2011; in revised form January 29, 2012)

Co-based ODS alloys, strengthened by nanosized oxide dispersion and γ′ precipitates, are potential high-temperature structural materials. The characteristics of the mechanically alloyed powder and the microstructural evolution of the Co-based ODS alloys were investigated. The results revealed that mechanical alloying had induced the formation of supersaturated solid solution in immiscible Co-Al-W-based alloys, originating mainly from extensive grain boundary region, high dislocation density, and ample point defect. Chemical compositions of mechanically alloyed Co-Al-W-based ODS alloys easily deviate from the γ/γ′ two-phase region, leading to the existence of Al_xCo, Co_3W, Co_7W_6, and W phases in addition to the γ and γ′ phases. Nonuniform distribution of alloying elements brings about the differences in morphologies and sizes of γ′ precipitates. Microstructural formation process is impelled by spinodal decomposition mode, and spinodal decomposition behavior has been accelerated in the fine-grained alloy because of the presence of short-circuited diffusion paths for atomic movement.

Keywords cobalt-based alloy, mechanical alloying, microstructure, oxide dispersion strengthening, spinodal decomposition

1. Introduction

The development of Co-based ODS alloys has been driven by the increasing high demand for high-temperature structural materials used in aerospace and power-generation industries (Ref 1). Conventional Co-based alloys exhibit reduced strength and ductility at high temperature because of the coarsening or dissolution of carbides (Ref 2). Novel Co-based ODS alloys strengthened by γ′ precipitates and oxide dispersion opens the possibility to extend both the intermediate and high-temperature strength limits of the Co-based alloys (Ref 3-5). γ′ precipitation hardening is considered to be more effective at intermediate temperature, while oxide dispersion strengthening further enhances the high-temperature mechanical properties by the dispersion of thermally stable oxides (Ref 6-8). Owing to the low stability of the ordered intermetallic phase (Co_3Ta, Co_3Ti), precipitation hardening mechanism has not been applied to the Co-based alloy until the discovery of stable $Co_3(Al,W)$ phase with $L1_2$ structure by Sato et al. (Ref 9, 10). The $Co_3(Al,W)$ phase results in high mechanical properties of Co-based alloy, rendering it as an interesting strengthening phase for further alloy development.

Lin Zhang, Xuanhui Qu, Xinbo He, Rafi-ud Din, Hengsan Liu, and **Mingli Qin**, State Key Laboratory for Advanced Metals and Materials, Beijing Key Laboratory for Powder Metallurgy and Particulate Materials, University of Science and Technology Beijing, Beijing 100083, People's Republic of China; and **Lin Zhang** and **Hongmin Zhu**, School of Metallurgical and Ecological Engineering, University of Science and Technology Beijing, Beijing 100083, People's Republic of China. Contact e-mail: quxh@ustb.edu.cn.

Mechanical alloying (MA) is a main technique employed to synthesize the advanced ODS alloys. MA plays an important role on the microstructure formation and the resulting properties. The novel Co-Al-W-based ODS alloys, synthesized by MA, exhibit the unique microstructural evolution which is much different from that of the conventional fusion metallurgical technology. It is generally accepted that the components of Al and W in Co-Al-W alloy can hardly dissolve into cobalt matrix except at high temperature (Ref 11, 12). However, the MA of immiscible Co-Al-W-based alloys induces the formation of nanocrystalline microstructure as well as supersaturated solid solution. With respect to the nanocrystalline nature, this phenomenon may be ascribed to the alteration in the free energy of the system and the diffusion paths caused by the surface energy contributions and the ultrafine grain structure resulting in a significant transformation in the metallurgical phase. On the other hand, with regard to the supersaturated solid solution, the highly non-equilibrium states and various kinds of non-equilibrium phase transformation or chemical reactions are the factors which result in complex microstructural evolution (Ref 13). Ukai and co-workers (Ref 14) have proposed the spinodal decomposition mechanism to explain the microstructural formation in Co-Al-Y_2O_3 alloy. The Co-Al-W system is an attractive alloy owing to the formation of $Co_3(Al,W)$ precipitates. It is found that the variations in composition and heat-treatment parameters induce the microstructural transformation, thus exerting a significant influence on the mechanical properties. To the best of our knowledge, until now, there is no research about the preparation of Co-Al-W alloys by MA method, and the phase formation mechanism by this method is still not comprehended well. Therefore, it is worth studying the evolution of microstructure to comprehend the spinodal mechanism. Furthermore, we also present a plausible explanation about the formation of γ′ precipitates. Moreover, we also elaborate the effects of nanocrystalline grains on the evolution of microstructure in Co-Al-W ball-milled alloys.

In the present study, a family of novel Co-Al-W-based ODS alloys has been synthesized exhibiting the dispersion of γ′

precipitates and extremely fine oxides. Particular emphasis is placed on the evolution of the microstructure obtained by MA and subsequent heat treatment. This information does not only show the possibility of utilizing the new γ' phase as strengthening phase in novel Co-based ODS alloys but also provides a basic understanding of the immiscible alloys fabricated by MA.

2. Experimental

Four kinds of alloys were designed, and the compositions are listed in Table 1. In order to adjust the volume fraction of γ' precipitates, the alloys with varying concentrations of Al and W were prepared. Above alloys were mechanically alloyed in a high energy planetary ball mill at a rotation speed of 400-480 rpm with the ball/powder weight ratio of 10:1 in Ar atmosphere for 60 h. The alloys were consolidated by spark plasma sintering (SPS) at 1145 °C. The specimens were solution treated at 1300 °C for 6 h and aged at 700-900 °C for 24 h.

Phase transformation was studied using Siemens D 5000 X-ray diffraction meter using Cu radiation. The polished specimens were etched with the solution of 30% HNO_3 + 70% CH_3OH. A LEO1450 SEM was utilized to characterize the microstructure. Microhardness was measured on V1000 using a load of 300 g. transmission electron microscope (TEM) specimens of the MA powder was made by embedding the powder in copper through electroless plating, followed by grinding and ion thinning. Subsequently, the specimens were observed using JEM 200 TEM equipped with energy dispersive X-ray spectroscopy (EDS).

Table 1 Chemical compositions of the designed alloys

Alloy designation	Al		W		Y_2O_3	Hf	
	at.%	wt.%	at.%	wt.%	wt.%	wt.%	Co
9Al	9	3.6	0	0	1.0	1.5	Bal.
7.5W	9	3.7	7.5	21.1	1.0	1.5	Bal.
10W	9	3.6	10	26.8	1.0	1.5	Bal.
12Al	12	5.1	7.5	14.8	1.0	1.5	Bal.
5W	9	3.9	5	14.8	1.0	1.5	Bal.

3. Results and Discussion

3.1 Formation of Supersaturated Solid Solution

Figure 1(a) shows the cross-sectional microstructure of MA powder. It exhibits typical feature of severe plastic deformation, which is ascribed to the repeated fracture and cold welding of powder mixture. The cold-welding process is considered to be dominant because the final particle size (20-60 μm) is much larger than original cobalt powder (1-2 μm). It is obvious that single particle actually consists of a large number of layer-shaped grains. The white particles are found to be undissolved W. Figure 1(b) shows HRTEM image of the milled powder. Both crystallite area and amorphous area can be differentiated, marked as C and A, respectively. The residual W is also marked in Fig. 1(b). No obvious oxide particles are differentiated, and it is considered that initial Y_2O_3 particles are dissolved by super heavy plastic deformation.

Figure 2 depicts the XRD patterns of the mixture milled for 60 h. It is vividly discernible that the diffraction peaks are broadened. The peak of Al cannot be detected, indicating that cobalt matrix has become supersaturated with Al. The relatively high peak of W maintains its position, which is attributed to its

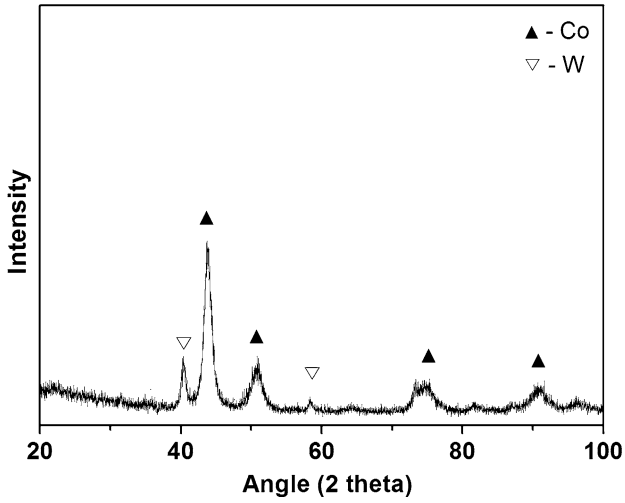

Fig. 2 XRD patterns of Co-based ODS alloy milled for 60 h

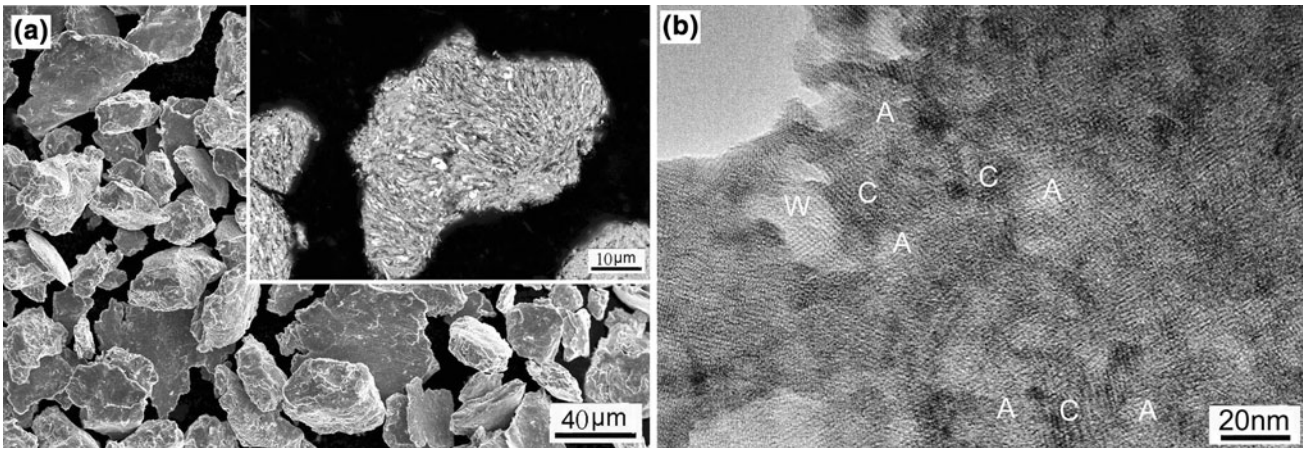

Fig. 1 Morphology of mechanically alloyed powder (a), and corresponding HRTEM image (b)

high concentration. Moreover, the higher solubility of Al in cobalt matrix also restricts the solubility of W (Ref 15).

Figure 3 summarizes the variations in crystalline size and microhardness as a function of milling time. On the one hand, crystalline size monotonically decreases from 204 nm to about 52 nm in the first 15 h, resulting in high interfacial energy. On the other hand, the hardness greatly increases and reaches the level of 590 Hv in the first 15 h, and it remains at about 640 Hv. The dislocation density calculated from the strain reaches up to 5.6×10^{16} m^{-2} for the alloys milled for 60 h.

The formation of supersaturated solid solution may be ascribed to two reasons. First, Al and W cannot be dissolved in cobalt matrix because of its extremely low solubility at room temperature (Ref 11, 12). The increase in surface energy due to refining of the components (Co, Al, W, and Y_2O_3) by super heavy plastic deformation supplements the driving force for the formation of supersaturated solid solution. Second, nanosized grains induce the formation of special grain boundary amorphous layer and complex wavy interfaces (Ref 16, 17). It is noted that main boundaries in nanocrystalline alloys prepared by MA are predominantly high angle grain boundaries, which exhibit a relatively open structure and large free volume. The bonds between the atoms in these high angle grain boundaries are found to be broken (Ref 13). The atoms residing at the grain boundary regions will therefore have lower energy as compared to that of the atoms within the grains. It is supposed that only some of the solute atoms are dissolved into the lattice of the solvent as substitutional atoms, and the extra solute atoms are located mainly at boundary region as atomic clusters and grain boundary atoms. In addition, a large number of lattice distortions, defects, and dislocations are generated, which act as accommodation sites of decomposed atoms and undissolved elements (W). The formation of supersaturated solid solution brings about complex microstructural change during subsequent heat treatment (Ref 18-20).

3.2 Microstructure of Co-Based ODS Alloys

In order to examine the possibility to fabricate the γ′ phase-strengthened Co-based ODS alloys by MA method, four kinds of alloys with varying contents of Al and W are designed. Figure 4 shows the microstructures of the alloys that are subjected to solution at 1300 °C for 6 h and subsequently aged at 900 °C for 24 h. In the case of 7.5W alloy, a high population of white precipitate gets distributed in the matrix, and a few large particles have been observed, as depicted in Fig. 4(a).

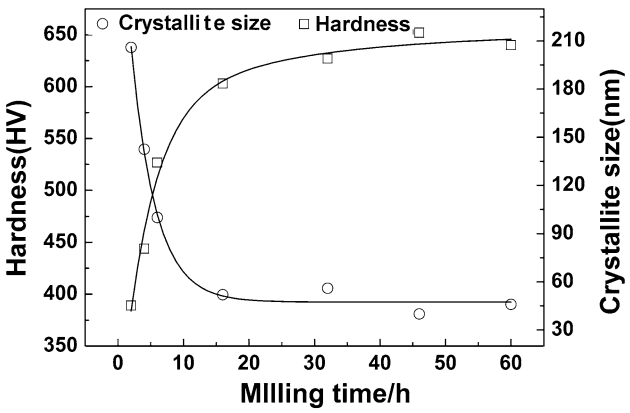

Fig. 3 Variations of hardness and grain size with milling time

Average size of the white precipitates is about 0.5 μm. Figure 4(b) presents the microstructure of 10W alloy. It is evident that the white particles are homogeneously distributed. The population of particles and the particle size are larger than those of 7.5W alloy. In addition, the precipitation-free area is visible in the inserted image of Fig. 4(b). Figure 4(c) clearly depicts that 5W alloy exhibits some white blocks, besides the fine precipitates. The microstructure of 12Al alloy displays remarkable coarsening, as shown in Fig. 4(d). The number of large white blocks has increased compared to that of 5W alloy and the large particles gradually decomposed into small white precipitates, as demonstrated in Fig. 4(d).

Figure 5 shows the XRD patterns of four types of Co-based ODS alloys. XRD results revealed the existence of Al_xCo, Co_3W, Co_7W_6, and W phases in addition to the γ and γ′ phases. The intensity of γ′ phase is the highest for 7.5W alloy, and the peaks of Co_3W, Al_xCo, Co_7W_6, and W are much lower than the other three kinds of alloys. In the case of 12Al alloy, the peaks of Al_xCo and $Y_5Al_3O_{12}$ are the strongest, suggesting that high content of Al promote the formation of Al_xCo phase and Y-Al-O complex oxides. The presence of Al_xCo and Co_3W implies the existence of phase decomposition, which will be discussed below.

Figure 6 shows the microstructures of 5W alloy aged for 24 and 48 h. The sample aged for 24 h shows nonuniform microstructure, and the microstructure exhibits a few large precipitates. Aging for 48 h yields an almost homogeneous distribution of white phase with only small amount of large precipitates, suggesting that the decomposition of large particles continues with an increase in the aging time.

Figure 7 presents the influence of aging temperature on the morphology of white precipitates in 7.5W alloy. In the case of the solution state, a small amount of white precipitates are visible, indicating that the white precipitates cannot be dissolved completely even under 1300 °C, as shown in Fig. 7(a). It is evident from Fig. 7(b) that the sample aged at 700 °C exhibits no obvious change in the particle size of white precipitates in comparison to that of the solutionized state. With the increasing of aging temperature, growth and coagulation of white precipitates take place. Aging at 800 °C leads to a vivid increase in particle size and population of white precipitates, as shown in Fig. 7(c). At the aging temperature of 900 °C, the volume fraction of white precipitates is estimated to be 45% with uniform distribution, as depicted in Fig. 7(d). The size of white precipitates increases from 0.48 to 0.62 μm in the temperature range of 700-900 °C, indicating that the white phase is a relatively stable phase.

3.3 Discussion

It is worth noting that the microstructure of Co-based ODS alloys fabricated by MA is much different from that of the cast Co-Al-W-based alloys developed by Sato et al. (Ref 10). Theoretically, γ/γ′ two-phase microstructure should be obtained, and no secondary phase was formed in alloy Co-9Al-10W (at.%, baseline alloy), but XRD analysis revealed the presence of various kinds of secondary phases. The detailed microstructure of Co-based alloys was further investigated to gain better understanding on the formation mechanisms of the microstructure. Figure 8 shows the high magnification microstructure of Co-based ODS alloys solutionized at 1300 °C for 6 h and aged at 800 °C for 24 h. In the case of 9Al alloy, two different contrasting regions can be obviously viewed: a dark

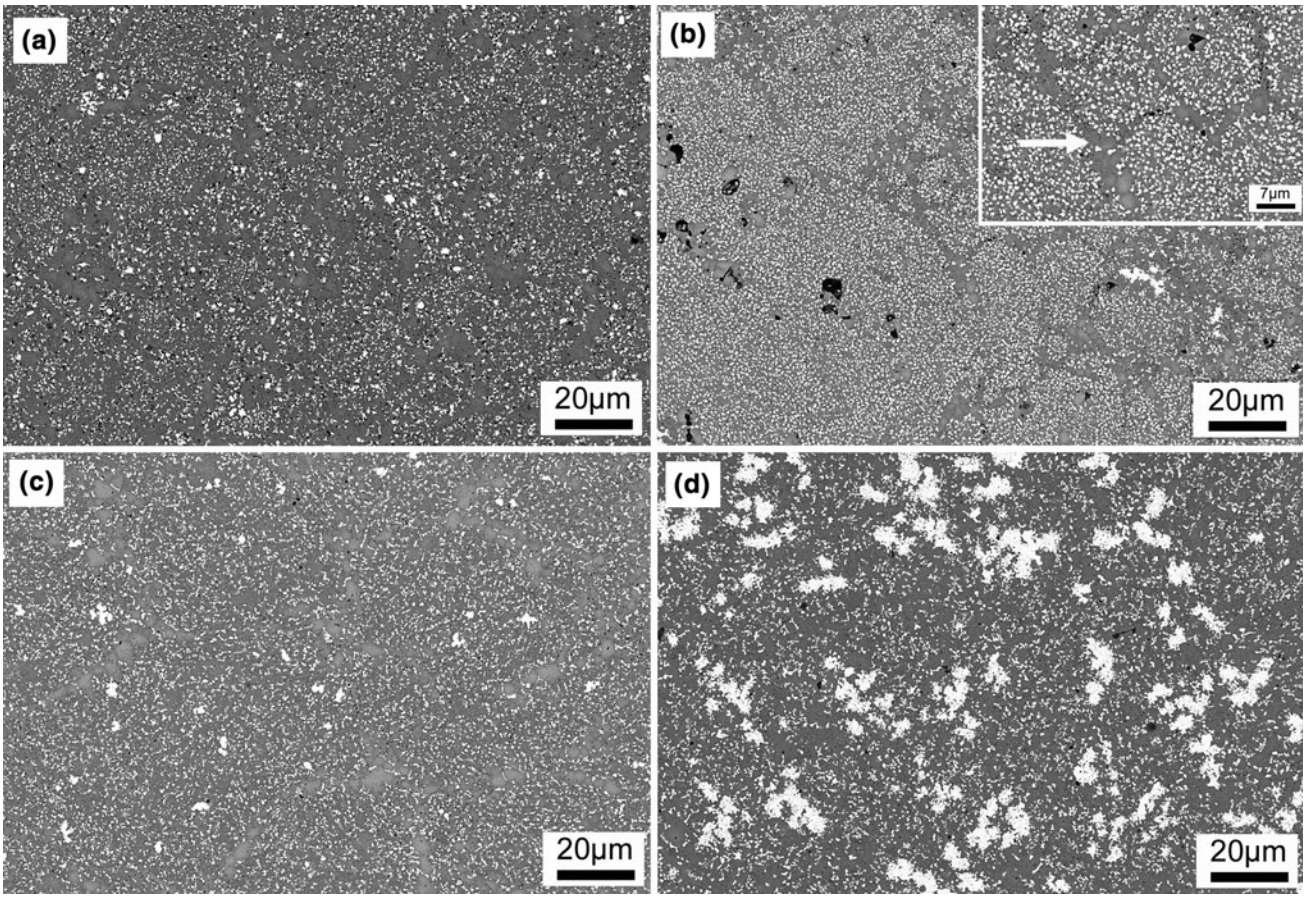

Fig. 4 SEM micrographs of four kinds of alloys aged for 24 h: (a) 7.5W, (b) 10W, (c) 5W, and (d) 12Al

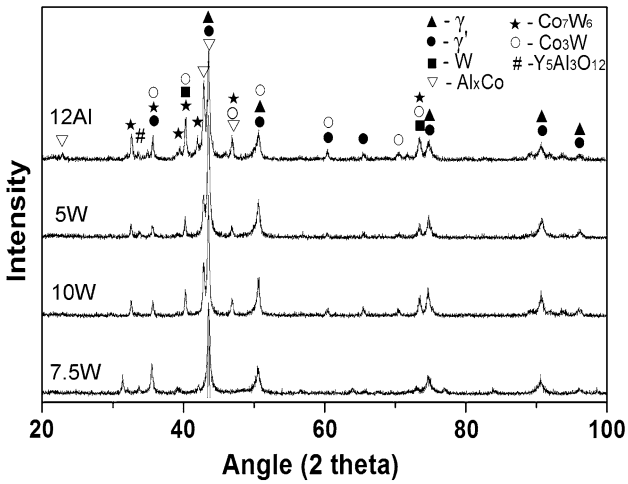

Fig. 5 XRD patterns of four kinds of Co-based ODS alloys

gray region (marked by the arrow), and a light gray region (marked by L). It is noted that the dark gray region is distributed along the boundaries of the light gray region, which is similar to the distribution of liquid film during liquid-phase sintering. The inserted image shown in Fig. 8(a) is the high magnification secondary electron image of the area marked by the frame. It is seen that a high population of gray spherical precipitates were formed in the light gray region, while few spherical particles were observed in the black region. As for 10W alloy, nonuniform distribution of the white precipitates was observed, as shown in Fig. 8(b). A large number of extremely fine white particles with the size of 0.22 μm were formed in the area marked by 1, as shown in the inserted image. Figure 8(c) exhibits the high magnification image of the region marked by 2. Relatively large blocky and plate-like precipitates were formed. It is indicated in Fig. 8(d) that three kinds of contrasting phases were present in the microstructure of 7.5W alloy: a white contrast phase (marked by C), a black contrast phase (marked by D), and a gray contrast phase (marked by E). In addition, the regions showing nearly no precipitates are called smooth region, marked as S in Fig. 8(d).

The EDS results of varied phases present in Fig. 8 are given in Table 2. It is revealed that the gray spherical particles observed in the inserted image of Fig. 8(a) are Al-rich phase with Al content as high as 18.5 at.%, which is much higher than the nominal concentration of Al (9 at.%) in 9Al alloy. Therefore, the composition fluctuation of Al in cobalt matrix builds up, implying the spinodal decomposition of the super-saturated solid solution of the Co-based ODS alloy. It is noted that these Al-rich particles cannot be suppressed even during rapid quenching process, suggesting the high tendency to precipitate. Referring to the XRD and EDS result, the spherical particles was Al_xCo phase. The content of W in the large block particle marked by A in Fig. 8(b) reached 72.5 at.%, indicating very limited diffusion between the particles with the matrix. The particle with extremely high W content inherited from the undissolved tungsten after MA. The content of W in the plate-like phase marked by B in Fig. 8(c) was 45.75 at.%, which is

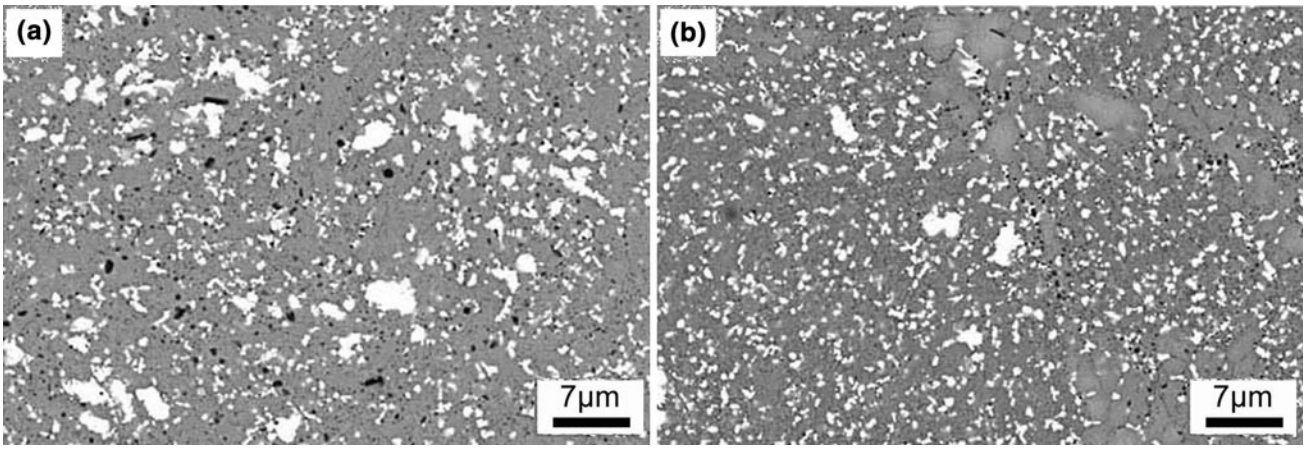

Fig. 6 SEM microstructure of 5W alloy aged for various times: (a) 24 h and (b) 48 h

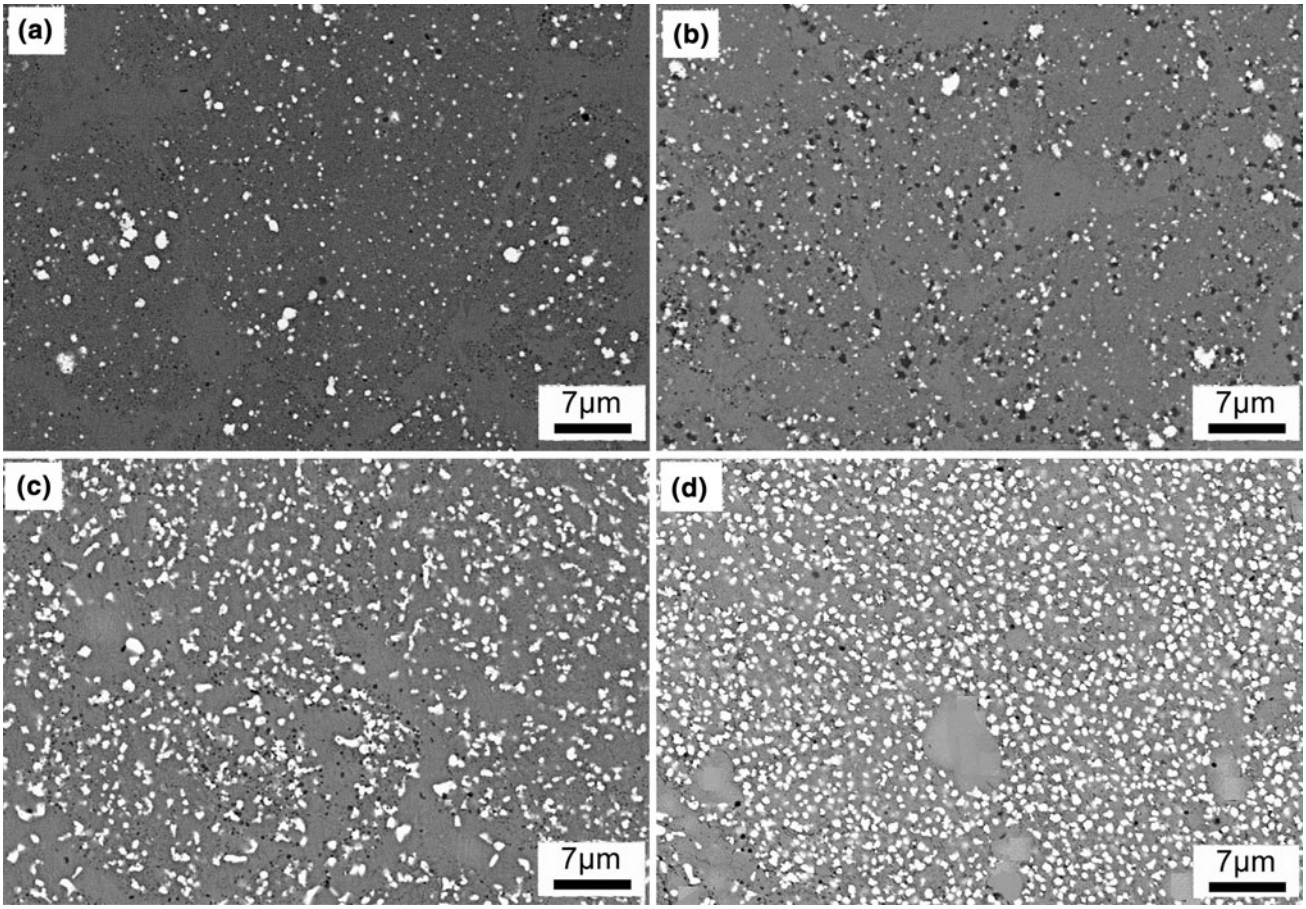

Fig. 7 SEM microstructures of 7.5W alloy solution-treated at 1300 °C for 6 h (a) and aged at varied temperatures: (b) 700 °C, (c) 800 °C, and (d) 900 °C

close to that of μ phase (Co_7W_6). Combined with the XRD results, the plate-like phase was identified as Co_7W_6-based μ phase. The small white precipitates (marked as C in Fig. 8d) contains 23.77 at.% W, which is much lower compared with the μ phase. These small white precipitates were identified as DO_{19} phase (Co_3W) by the combination of XRD analysis and EDS results. The black precipitates (marked as D in Fig. 8d) contains 29.99 at.% Al, which is Co_xAl-based phase. The gray phase marked as E (Fig. 8d) should be γ′ precipitates, which can be confirmed by the following data.

Figure 9 shows the microstructure of the 7.5W alloy etched by the solution of 100 ml ethanol, 10 ml HCl, and 5 g $CuCl_2$. In comparison to the microstructure shown in Fig. 8, the W-enriched phases (Co_7W_6, Co_3W, and W) were removed and the characteristics of γ′ phase can be clearly observed. The distribution of γ′ precipitates is indicated in Fig. 9(a). The largest

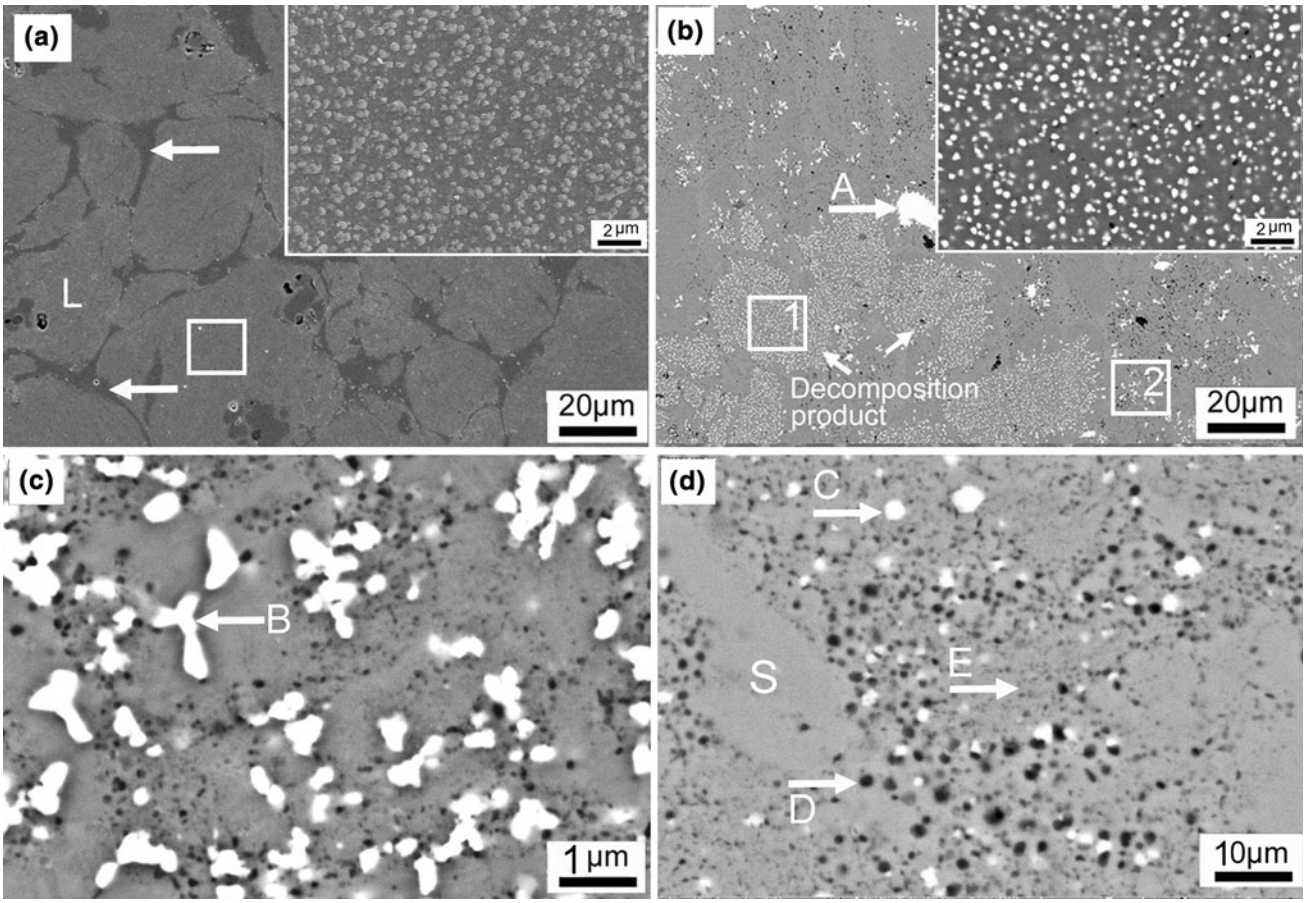

Fig. 8 SEM microstructures of varied alloys solution-treated at 1300 °C for 6 h and aged at 800 °C for 24 h: (a) 9Al, (b, c) 10W, and (d) 7.5W

Table 2 EDS results of varied phases in Co-Al-W-based ODS alloys (at.%)

Region	Phase	Co	Al	W
Spherical precipitates (Fig. 8a)	Co_xAl	80.68	18.5	-
A (Fig. 8b)	W	18.85	8.66	72.5
B (Fig. 8c)	Co_7W_6	47.55	6.70	45.75
C (Fig. 8d)	Co_3W	72.28	2.99	23.77
D (Fig. 8d)	Co_xAl	66.96	29.99	3.06

γ′-formed area is marked by A, as shown in Fig. 9(a). There is nearly no existence of W-enriched phases in region A, which corresponds to the smooth region shown in Fig. 8(d). Meanwhile, sporadic distribution of γ′ precipitates was observed in the other regions, which coexists with the W-enriched phases. Figure 9(b) shows the high magnification secondary electron image of the region marked by the white frame observed in Fig. 9(a). These precipitates exhibit typical morphology of γ′ phase. The size of γ′ precipitates was not homogeneous. Ultrafine spherical γ′ precipitates with the average size of 0.21 μm, relatively large cuboidal γ′ precipitates (0.39 μm), and large irregular γ′ precipitates (0.9 μm) were observed. This is attributed to the nonuniform distribution of alloying elements. The nonhomogeneous composition of γ′ phase induced different lattice mismatch between γ′ precipitates and the matrix, resulting in the variance of morphology and particle size.

In order to further certify the formation of γ′ precipitate, the TEM image of 7.5W alloy was investigated. Figure 10 presents the TEM images of 7.5W alloy. The precipitation of γ′ phase is clearly observed, and the oxide dispersions are distributed in both the γ matrix and the γ′ phase, as indicated in Fig. 10(a) and (b). Figure 10(c) and (d) shows the corresponding selected area electron diffraction (SAED) patterns presenting the (110) reflection that justifies the presence of γ′ precipitates.

It is seen from the isothermal section of the Co-Al-W ternary system that the γ/γ′ two-phase region is very small (Ref 10). MA induced the formation of supersaturation solid solution, but not the completely alloyed powder. It is the formation of supersaturation solid solution that brings about complex microstructural evolution. The alloying compositions easily deviate from the γ/γ′ two-phase region, resulting in the formation of various kinds of secondary phases. It is suggested from the Co-Al phase diagram that liquid phase may form through a series of reactions (Ref 11):

$$(\mathrm{Al}) + \mathrm{Al_9Co_2} \leftrightarrow \mathrm{L}(657\,^{\circ}\mathrm{C}) \quad \text{(Eq 1)}$$

$$\mathrm{Al_9Co_2} \rightarrow \mathrm{L} + \mathrm{Al_{13}Co_4}(970\,^{\circ}\mathrm{C}) \quad \text{(Eq 2)}$$

$$\mathrm{Al_{13}Co_4} \rightarrow \mathrm{L} + \mathrm{Al_3Co}\ (1093\,^{\circ}\mathrm{C}) \quad \text{(Eq 3)}$$

$$\mathrm{Al_3Co} \rightarrow \mathrm{L} + \mathrm{Al_5Co_2}(1135\,^{\circ}\mathrm{C}) \quad \text{(Eq 4)}$$

It is proposed that liquid phase was formed during consolidation, and the amount of liquid phase increases with

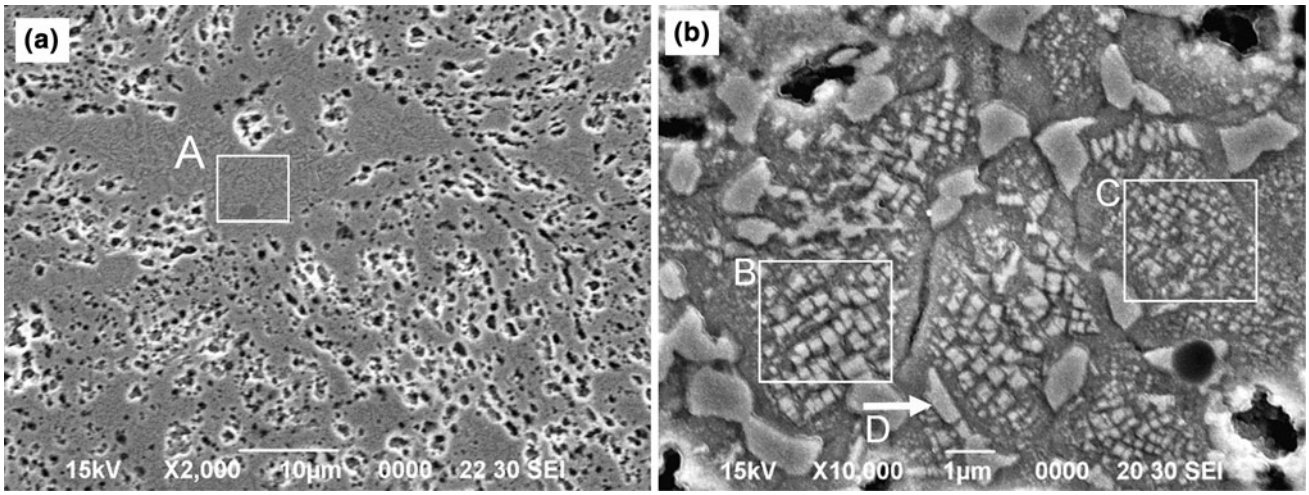

Fig. 9 SEM microstructures of 7.5W alloys solution-treated at 1300 °C for 6 h and aged at 900 °C for 24 h

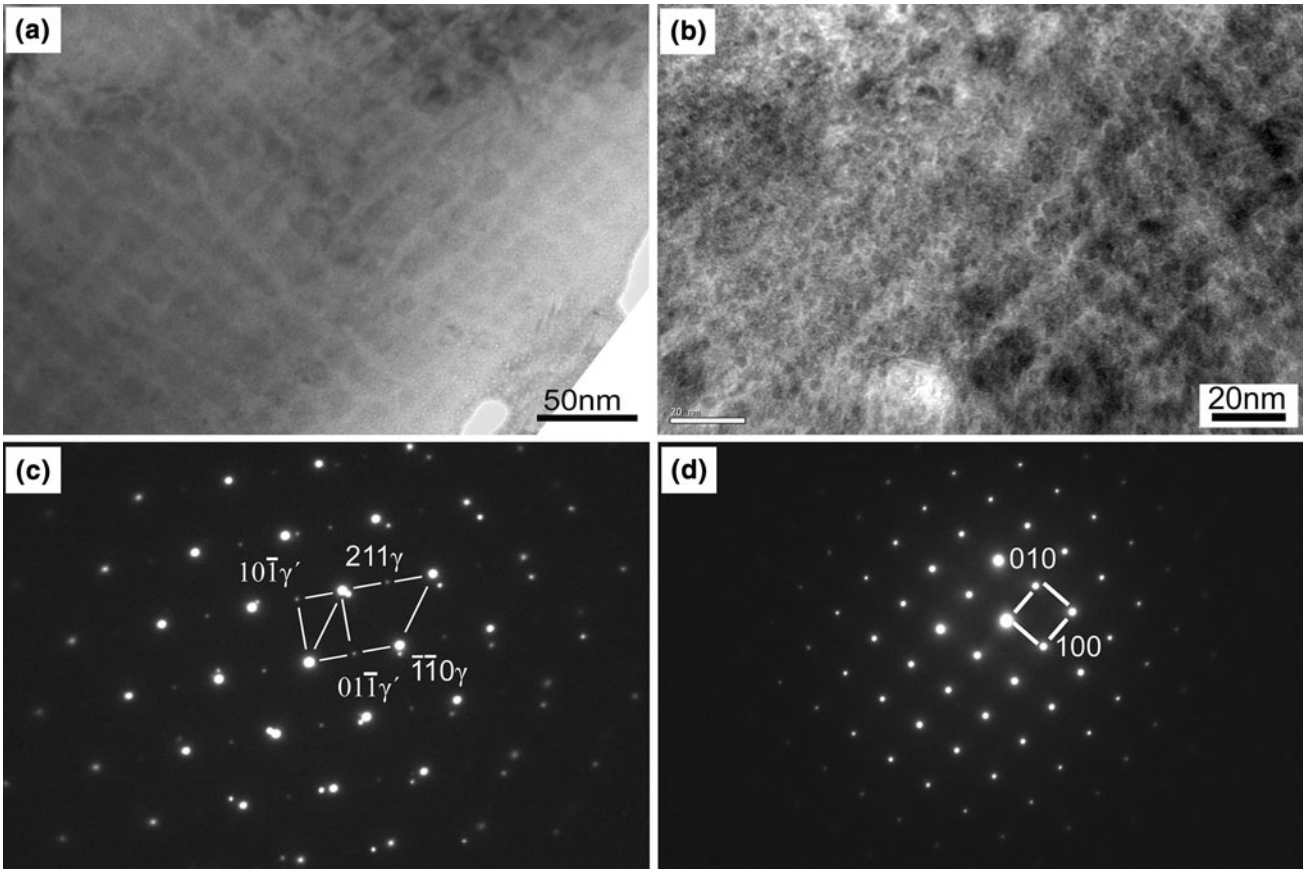

Fig. 10 TEM images of 7.5W alloy showing γ′ precipitates (a, b) and the SAED patterns of (c) γ′ precipitates; (d) γ matrix

increasing temperature. The liquid phase migrates along the prior powder particle under pressure, facilitating the rearrangement of neighboring particles and enhancement of densification. The liquid film is repelled because of the significant reduction of solubility of Al and W during solidification process. This behavior begets the preferential accumulation of liquid phase at the particle boundaries and the triple junctions after solidification. The precipitation-free area observed in Fig. 4(b) and the dark gray area observed in Fig. 8(a) serve as the proof of this hypothesis. Since the formation of liquid phase enhanced the solubility of W in the liquid phase, it is highly possible that the composition of liquid phase located within the γ/γ′ eutectic region, leading to the precipitation of γ′ phase after solidification. In the other regions, liquid phase is not involved, and solid phase reaction may be the dominant mode. Because the supersaturated solid solution is in a non-equilibrium state and it decomposes spinodally, short-range compositional fluctuations of Al and W progressively build up (Ref 12-21). The

decomposed products of Co_xAl and Co_3W have already been verified by XRD results (Fig. 5). The white particles and black particles marked in Fig. 8(a) and (b) represents the precipitations of Co_xAl and Co_3W, respectively, through spinodal decomposition mechanism. This decomposition behavior renders great contribution to the microstructural evolution. It is indicated that the decomposition process proceeds, and more stable γ' phase is formed through the reaction (Ref 15):

$$\gamma + CoAl + Co_3W \rightarrow ' \quad \text{(Eq 5)}$$

γ' precipitates can only be formed in local area that meets the composition requirement of γ' phase. The distribution of W-enriched phase is confined interior of the MA particle because of its low diffusion coefficient, and it is not involved in the formation of liquid phase. It is worth noting that ultrafine grains are formed because of the pinning of oxide dispersion and γ' precipitates (Ref 22). The large fraction of grain boundary regions provides the short-circuited diffusion paths for atomic movements, which is favorable for the decomposition process and the chemical order-disorder transformation (Ref 23). The mechanism controlling the size of γ' phase and its formation mechanism need to be further investigated. Enhancement of the solubilities of Al and W in cobalt matrix is an important challenge to promote the precipitation of γ' phase and restrict the formation of secondary phases.

4. Conclusions

Microstructural characterization of the MA powder and the fabricated Co-based ODS alloys was performed, and the following conclusions can be drawn:

(a) Supersaturated solid solution was formed in mechanically alloyed Co-Al-W-based ODS alloys, originating mainly from extensive grain boundary region, high dislocation density, and ample point defect.
(b) Chemical compositions of the Co-Al-W-based ODS alloy easily deviate from the γ/γ' two-phase region, leading to the existence of Al_xCo, Co_3W, Co_7W_6, and W phases in addition to the γ and γ' phases. Nonuniform distribution of alloying elements brings about the difference in morphology and size of γ' precipitates.
(c) Microstructural formation process is impelled by spinodal decomposition mode, and spinodal decomposition behavior has been accelerated in the fine-grained alloy because of the presence of short-circuited diffusion paths for atomic movement.

Acknowledgments

The research was financially supported by the National Nature Science Foundation of China (51104007), and the National Postdoctoral Foundation of China (20100480198, 1104053). The authors greatly thank S. Ukai from Hokkaido University for his direction on ODS alloys.

References

1. C.F. Tang, F. Pan, X.H. Qu, C.C. Jia, and B.H. Duan, Spark Plasma Sintering Cobalt Base Superalloy Strengthened by Y-Cr-O Compound Through High-Energy Milling, *J. Mater. Process. Technol.*, 2008, **204**, p 111–116
2. S.H. Zangeneh and H. Farhangi, Influence of Service-Induced Microstructural Changes on the Failure of a Cobalt-Based Superalloy First Stage Nozzle, *Mater. Des.*, 2010, **31**, p 3504–3511
3. L. Zhang, S. Ukai, T. Hoshino, S. Hayashi, and X.H. Qu, Y_2O_3 Evolution and Dispersion Refinement in Co-Base ODS Alloys, *Acta Mater.*, 2009, **57**, p 3671–3682
4. A. Wasilkowska, M. Bartsch, U. Messerschmidt, R. Herzog, and A. Czyrska-Filemonowicz, Creep Mechanisms of Ferritic Oxide Dispersion Strengthened Alloys, *J. Mater. Process. Technol.*, 2003, **133**, p 218–224
5. K. Shinagawa, T. Omori, K. Oikawa, and R. Kainuma, Ductility Enhancement by Boron Addition in Co-Al-W High-Temperature Alloys, *Scr. Mater.*, 2009, **61**, p 612–615
6. M. Nganbe and M. Heilmaier, Modelling of Particle Strengthening in the γ' and Oxide Dispersion Strengthened Nickel-Base Superalloy PM3030, *Mater. Sci. Eng. A*, 2004, **387–389**, p 609–612
7. L.J. Park, H.J. Ryu, S.H. Hong, and Y.G. Kim, Microstructure and Mechanical Behavior of Mechanically Alloyed ODS Ni-Base Superalloy for Aerospace Gas Turbine Application, *Adv. Perform. Mater.*, 1998, **5**, p 279–290
8. M. Nganbe and M. Heilmaier, High Temperature Strength and Failure of the Ni-Base Superalloy PM 3030, *Int. J. Plast.*, 2009, **25**, p 822–837
9. K. Shinagawa, T. Omori, J. Sato, K. Oikawa, and I. Ohnuma, Phase Equilibria and Microstructure on γ' Phase in Co-Ni-Al-W System, *Mater. Trans.*, 2008, **49**, p 1474–1479
10. J. Sato, T. Omori, K. Oikawa, I. Ohnuma, R. Karinuma, and K. Ishida, Cobalt-Base High-Temperature Alloys, *Science*, 2006, **312**, p 90
11. K. Niitsu, T. Omori, M. Nagasako, and K. Oikawa, Phase Transformations in the B_2 Phase of Co-rich Co-Al Binary Alloys, *J. Alloys Compd.*, 2011, **509**, p 2697–2702
12. G. Östberg, B. Jansson, and H.O. Andrén, On Spinodal Decomposition in the Co-W System, *Scr. Mater.*, 2006, **54**, p 595–598
13. C. Bansal and S. Sarkar, Phase Transformations in Nanocrystalline Alloys Synthesized by Mechanical Alloying, *J. Mater. Sci.*, 2004, **39**, p 5023–5029
14. K. Takezawa, S. Ukai, and S. Hayashi, Microstructure Control of Co-Base ODS Alloys, *Adv. Mater. Res.*, 2011, **239–242**, p 864–867
15. S. Kobayashi, Y. Tsukamoto, T. Takasugi, and H. Chinen, Determination of Phase Equilibria in the Co-Rich Co-Al-W Ternary System with a Diffusion-Couple Technique, *Intermetallics*, 2009, **17**, p 1085–1089
16. Y. Kimura, H. Hidaka, and S. Takaki, Work-Hardening Mechanism During Super-Heavy Plastic Deformation in Mechanically Milled Iron Powder, *Mater. Trans.*, 1999, **40**, p 1149–1157
17. S. Takaki, K. Kawasaki, and Y. Kimura, Mechanical Properties of Ultra Fine Grained Steels, *J Mater. Process. Technol.*, 2001, **117**, p 359–363
18. H. Sakasegawa, S. Ohtsuka, S. Ukai, and H. Tanigawa, Particle Size Effects in Mechanically Alloyed 9Cr ODS Steel Powder, *J. Nucl. Mater.*, 2007, **367–370**, p 185–190
19. A. Suzuki and J.M. Pollock, High-Temperature Strength and Deformation of γ/γ' Two-Phase Co-Al-W-Base Alloys, *Acta Mater.*, 2008, **56**, p 1288–1297
20. A.M. Mebed and M.I. Abd-Elrahmany, Thermal Analysis Study for the Phase Determination and Instable to Metastable Transformation of the Co-13Cu Alloy, *Phase Transitions*, 2009, **82**, p 587–598
21. U. Czubayko, N. Wanderka, V. Naundorf, V.A. Ivchenko, A.Y. Yermakov, M.A. Uimin, and H. Wollenberger, Three-Dimensional Atom Probing of Supersaturated Mechanically Alloyed Cu-20at.% Co, *Mater. Sci. Eng. A*, 2002, **327**, p 54–58
22. P. Grahle and E. Arzt, Microstructural Development in Dispersion Strengthened NiAl Produced by Mechanical Alloying and Secondary Recrystallization, *Acta Mater.*, 1997, **45**, p 201–211
23. M. Zhu, X.Z. Che, and Z.X. Li, Mechanical Alloying of Immiscible Pb-Al Binary System by High Energy Ball Milling, *J. Mater. Sci.*, 1998, **33**, p 5873–5881